Multihorizon Model Predictive Control: An Application to Integrated Power and Thermal Management of Connected Hybrid Electric Vehicles

Qiuhao Hu, Mohammad Reza Amini, Ilya Kolmanovsky, *Fellow, IEEE*, Jing Sun, *Fellow, IEEE*, Ashley Wiese, and Julia Buckland Seeds

***Abstract*— In this article, we propose a multihorizon model predictive control (MH-MPC) approach with applications to integrated power and thermal management (iPTM) of connected hybrid electric vehicles (HEVs). The proposed MH-MPC leverages preview and optimization over a short receding and a long shrinking horizon, where the accuracy of preview, model, and integration can be different over different horizons. Compared with a conventional MPC-based approach with a short prediction horizon and terminal cost, the MH-MPC improves fuel consumption to a level comparable to dynamic programming (DP) while still being computationally affordable. A statistical sensitivity analysis over real-world city driving cycles is conducted to demonstrate the robustness of MH-MPC to moderate levels of uncertainty in the long-term preview.**

***Index Terms*— Model predictive control (MPC), multitimescale optimization, power and thermal management (PTM).**

Nomenclature

C_{bat}	Battery capacity [A · h].
C_{eng}	Engine-specific heat capacity [J/kg · °C].
f_{fuel}	Nominal fuel consumption rate [kg/s].
LHV	Lower heating value [J/kg].
M_{eng}	Equivalent thermal mass [kg].
$\dot{m}_{\text{fuel}}$	Fuel consumption rate [kg/s].
P_{bat}	Battery power [W].
$P_{\text{bat}}^{\text{aux}}$	Battery power for auxiliary systems [W].
$P_{\text{bat}}^{\text{trac}}$	Battery power for traction [W].
P_{eng}	Engine power [W].
P_{trac}	Traction power [W].
$\dot{Q}_{\text{air}}$	Heat rate rejected by air convection [W].
$\dot{Q}_{\text{exh}}$	Heat rate rejected in the exhaust [W].
$\dot{Q}_{\text{fuel}}$	Heat rate released in combustion process [W].
$\dot{Q}_{\text{heat}}$	Heat rate exchanged for cabin heating [W].
R_{bat}	Battery resistance [Ω].
SOC	Battery state-of-charge [−].
R_{int}	Battery internal resistance [Ω].
T_{cl}	Engine coolant temperature [°C].
δt	Sampling time [s].
U_{oc}	Battery open-circuit voltage [V].
α	Multiplier of fuel consumption rate [−].
λ	Penalty weight [−].

Acronyms

BSFC	Brake-specific fuel consumption.
CAV	Connected and automated vehicle.
DP	Dynamic programming.
HEV/EV	Hybrid electric vehicle/electric vehicle.
HVAC	Ventilation and air conditioning.
iPTM	Integrated power and thermal management.
MPC	Model predictive control.
MH-MPC	Multihorizon model predictive control.
NEDC	New European driving cycle.
RPM	Round per minute.
V2I/V2V	Vehicle-to-infrastructure/vehicle.

Manuscript received September 17, 2020; revised March 30, 2021; accepted June 5, 2021. Manuscript received in final form June 21, 2021. This work was supported in part by the United States Department of Energy (DOE), ARPA-E NEXTCAR program under Award DE-AR0000797 for the University of Michigan portion. Recommended by Associate Editor L. Fagiano. *(Corresponding author: Mohammad Reza Amini.)*

Qiuhao Hu, Mohammad Reza Amini, and Jing Sun are with the Department of Naval Architecture and Marine Engineering, University of Michigan, Ann Arbor, MI 48109 USA (e-mail: qhhu@umich.edu; mamini@umich.edu; jingsun@umich.edu).

Ilya Kolmanovsky is with the Department of Aerospace Engineering, University of Michigan, Ann Arbor, MI 48109 USA (e-mail: ilya@umich.edu).

Ashley Wiese and Julia Buckland Seeds are with Ford Motor Company, Dearborn, MI 48124 USA (e-mail: awiese@ford.com; jbucklan@ford.com).

Color versions of one or more figures in this article are available at https://doi.org/10.1109/TCST.2021.3091887.

Digital Object Identifier 10.1109/TCST.2021.3091887

I. Introduction

MPC is of interest for a broad range of applications including mobility, transportation, and aviation systems [1]. For integrated systems, MPC has to exploit the complementary characteristics of individual components to achieve high performance. Many integrated processes have dynamics responding over different timescales. Such systems are common in chemical processes [2], [3], micro-grids [4], mining applications [5], electrified vehicles [6]–[8], and aircraft [9]. When MPC is applied to such multitimescale systems, the slower dynamics often dictate that a relatively long prediction horizon be used which leads to a large computational footprint. To address that issue, a commonly used

approach is to exploit the singular perturbation theory [10], in which a system with explicit timescale separation in the dynamics is decomposed into two reduced-order subsystems with different timescales, see [11]–[14]. Next, "fast" and "slow" MPCs are designed and applied to control fast and slow dynamics, respectively.

An alternative approach for dealing with multitimescale systems is hierarchical MPC (H-MPC) [7]–[9], [15]–[17]. Unlike the decentralized fast-slow MPC approach based on the singular perturbation theory that does not necessarily require communication between the slow and fast MPCs [12], an H-MPC computes the optimal reference values for the "slow" dynamics over a relatively long prediction horizon. Then, a tracking problem is solved over a much shorter prediction horizon to track the planned references and compute the control commands. Note that the tracking controller could be of PID type [18]. In our previous publications [7], [8], we developed an H-MPC with an economic MPC implemented in the top, scheduling layer, with a long prediction horizon and a long sampling period, and a tracking MPC as the lower, piloting layer. In this implementation, compared with scheduling-layer MPC, the tracking MPC is designed with a shorter horizon and a shorter sampling period. This H-MPC approach was demonstrated [7], [8] for integrated battery and cabin thermal management of electrified CAVs.

For the H-MPC framework in [7], [8], and [19], both scheduling and piloting MPCs were implemented using a receding horizon scheme. Despite the relatively long prediction horizon considered at the top layer of H-MPC, satisfying the terminal constraint at the end of the operation cannot always be guaranteed from the beginning. Such a design requirement is of great importance for mission-based applications, where a specific mission/task needs to be accomplished over a finite time duration while having access to a limited onboard energy resource. The developments in this article are motivated by an opportunity to tailor and improve strategies for MPC in such mission-based applications, which have to be accomplished over a finite time duration.

As an example, consider an energy management strategy for HEVs, where the objective is to minimize fuel consumption over the entire trip, subject to a battery charge sustainability constraint that needs to be enforced at the end of the mission (i.e., the trip). If a conventional receding horizon MPC with a finite horizon is used for energy management of HEVs, this battery charge sustainability constraint is often enforced by adding a terminal penalty on the deviation of the battery SOC from its reference value—which is often set to be a constant value—at the end of the prediction horizon [20], [21]. Given the finite horizon of the MPC, such a terminal penalty in the cost may limit the practical range of the battery SOC, forcing the HEV powertrain to operate in a narrow and less efficient region [22]. One approach to alleviate this issue is to precompute the optimal SOC references using offline optimization approaches (e.g., DP [23]) and design a finite horizon tracking MPC to follow the optimal trajectory. Such an approach is computationally expensive and requires prior knowledge about the entire vehicle speed profile and load trajectory. While significant efforts to develop approaches for forecasting these quantities are being made (see [24], [25] and the references therein), the long-term forecasts are typically inaccurate. The precomputed SOC references are often not robust to the uncertainties associated with the long-term vehicle speed preview, calling for an online SOC reference optimizer that responds to the feedback from the powertrain system and changes in the vehicle speed and traffic conditions in real-time.

In this article, a novel multihorizon model predictive control (MH-MPC) control strategy is proposed for mission-based problems. The approach combines a short receding horizon and a long shrinking horizon. The prediction over the short receding horizon can be performed with a shorter sampling period, exploiting more accurate preview information and models than over the shrinking horizon. The shrinking horizon cost essentially provides an approximation of the "cost-to-go" function/terminal cost from the end of the receding horizon to the end of the mission. Due to the possibility of using short and long sampling periods, such an approach can handle multitimescale dynamics. In this article, the application of the proposed MH-MPC framework is demonstrated for iPTM of HEVs.

Efficient thermal management of electrified vehicles, including that of the combustion engine, battery, exhaust aftertreatment, and cabin temperature, has a significant impact on the overall fuel economy and driving range. This is especially true in cold and hot ambient conditions [6], [26], [27], where: 1) the actuators used for thermal management (e.g., compressor, pumps, and fans) can consume a considerable amount of energy at the rate of up to 2.5 kW [28], [29] and 2) the efficiencies of the vehicular power and thermal systems degrade outside of the optimal temperature range. For HEVs, thermal management priority varies as the ambient temperature changes. In cold ambient temperature, which is the focus of this article, the main thermal loads are due to thermal management of the engine, and cabin heating is the main thermal load.

Fig. 1 shows the power and thermal loops of a common power-split HEV. As is seen from Fig. 1, a portion of the heat generated during the combustion process is absorbed by the engine coolant, while the rest of the fuel energy is converted to either mechanical work or wasted through the exhaust gases. If there is any demand for cabin heating, the stored thermal energy in the coolant is then used to heat the cabin air via the heater cores. As a result, cabin heating reduces the coolant temperature, forcing the engine to run to generate heat once the coolant temperature drops below a certain threshold (e.g., 40–50 °C [22], [30])—even if there is no demand for traction power.

The emergence of CAV technologies in recent years has provided unique opportunities to enhance situational awareness of the vehicle [25], [31], allowing for vehicle speed and road grade forecasting. Exploiting these forecasts for energy flow optimization has made MPC a natural choice for real-time iPTM of HEVs [32]. There are two main challenges in applying MPC to iPTM:

1) the coupling between power and thermal dynamics that respond over different timescales,

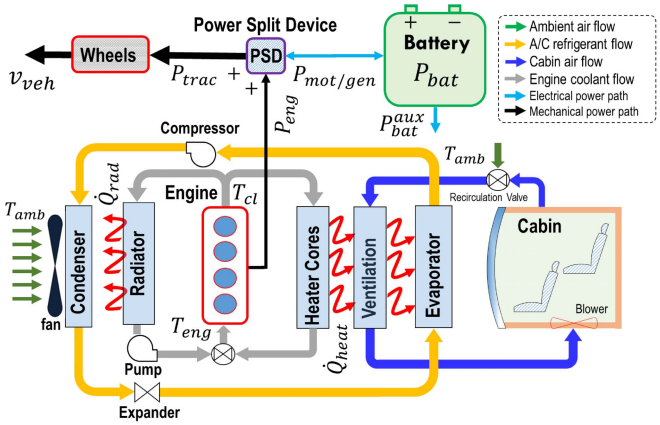

Fig. 1. Schematic of a power-split HEV with power and thermal loops.

2) uncertainties associated with vehicle speed forecast that can influence the MPC performance unfavorably.

Fig. 2 highlights the timescale separation between power and thermal systems of an HEV using the data collected from a test vehicle. As can be seen, the response of engine power [Fig. 2(b)] is relatively fast, for example, within 1–3 − s time constant. On the other hand, the engine coolant temperature [Fig. 2(c)], which represents the thermal dynamics of the combustion engine, responds much slower with a time constant in the order of 30 s. Despite responding over different timescales, the power and thermal dynamics are strongly coupled. Fig. 2 shows that when the engine is used to meet the driver traction power demand, the engine coolant temperature increases simultaneously.

The multitimescale dynamics and mission-based nature of an HEV operation motivate the use of the MH-MPC to facilitate energy management. To this end, in this article, MH-MPC is applied to address iPTM challenges in HEVs. We consider a wintertime condition with cold ambient temperature when cabin heating is required. In this scenario, and assuming that the destination is known, the objective of iPTM is to minimize fuel consumption while enforcing power and thermal constraints. MH-MPC was first introduced in our preliminary conference paper [22], in which the performance of the controller was evaluated over a limited number of standard driving cycles under the assumption of perfect knowledge of future vehicle speed. In this article, we extend our previous work by: 1) evaluating the MH-MPC performance over real-world urban driving cycles and performing statistical analysis for a large number of vehicles; 2) investigating the sensitivity of MH-MPC performance and computational footprint to the length and sampling periods used over the shrinking and receding horizons; and 3) assessing the MH-MPC robustness to uncertainties associated with vehicle speed prediction. Additionally, this article reports a variant of MH-MPC with details, discussions, and interpretations not available in [22].

The rest of this article is organized as follows: First, the physics-based and control-oriented models of the power and thermal systems of an HEV are introduced in Section II. Next, the design of MPC-based iPTM strategies is discussed in Section III, including the conventional MPC and the

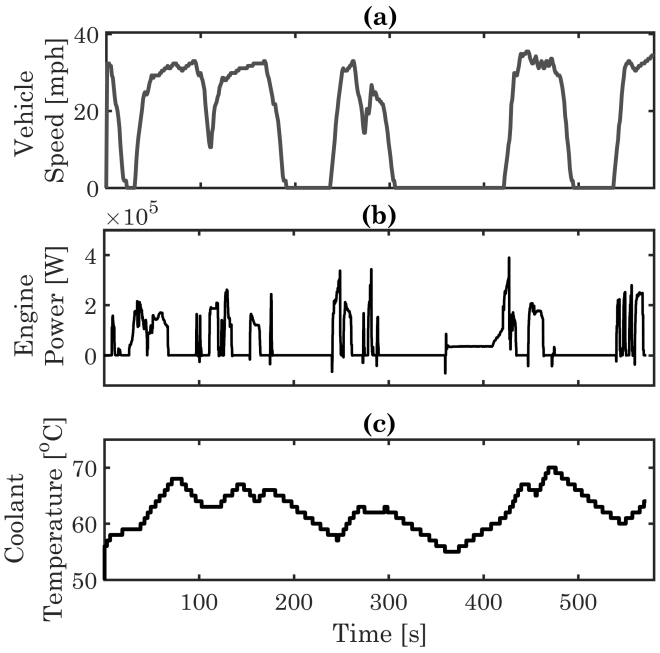

Fig. 2. Time-scale separation between power and thermal systems in an HEV: (a) vehicle speed, (b) engine power, and (c) engine coolant temperature. Data collected from a test HEV.

MH-MPC. Section IV presents the sensitivity analysis of the proposed MH-MPC to uncertainties in vehicle speed preview and discusses the MH-MPC robustness. Finally, concluding remarks are summarized in Section V.

II. Motivation Case Study: HEV Power and Thermal Models

We use the iPTM problem for HEV as a motivating example to, first, demonstrate the special controller design requirements for integrated systems with multitimescale dynamics and, second, show the need for a new MPC design, that is, MH-MPC, for such systems. For a HEV powertrain system, as shown in Fig. 1, the battery SOC and engine coolant temperature ($T_{\rm cl}$) dynamics represent the main dynamics in the power and thermal systems, respectively. The physics-based models of SOC and $T_{\rm cl}$ are introduced in Sections II-A and II-B. The details of the HEV model considered in this article are described in [6] and [30].

A. Battery Power-Balance Model

For a power-split HEV, the power provided by battery ($P_{\rm bat}^{\rm trac}$) and internal combustion engine ($P_{\rm eng}$) is blended to meet the traction power demand ($P_{\rm trac}$) for driving

$$P_{\rm trac} = P_{\rm bat}^{\rm trac} + P_{\rm eng}. \tag{1}$$

Additionally, the battery provides the power for auxiliary systems ($P_{\rm bat}^{\rm aux}$)

$$P_{\rm bat} = P_{\rm bat}^{\rm trac} + P_{\rm bat}^{\rm aux} \tag{2}$$

where $P_{\rm bat}$ is the total battery power. Note that for cold weather operation, the power required for the operation of the engine and cabin thermal management system's actuators

(e.g., electric coolant pump, radiator fan, HVAC blower) is considered as the main auxiliary load ($P_{\text{bat}}^{\text{aux}}$) on the HEV battery. The battery SOC dynamics are represented using an equivalent circuit model

$$\dot{\text{SOC}}(t) = f_{\text{SOC}}(t) = \frac{U_{\text{oc}} - \sqrt{U_{\text{oc}}^2 - 4R_{\text{int}}P_{\text{bat}}}}{2R_{\text{int}}C_{\text{bat}}} \tag{3}$$

where t denotes time, while C_{bat}, R_{int}, and U_{oc} are the capacity, internal resistance, and open-circuit voltage of the battery, respectively.

B. Engine Coolant Temperature Model

In cold ambient temperatures, thermal management of the engine and cabin heating are the main thermal loads. The thermal dynamics of engine coolant are modeled based on the energy balance [26]

$$\dot{T}_{\text{cl}}(t) = f_{T_{\text{cl}}}(t) = \frac{1}{M_{\text{eng}}C_{\text{eng}}} \times (\dot{Q}_{\text{fuel}} - P_{\text{eng}} - \dot{Q}_{\text{exh}} - \dot{Q}_{\text{air}} - \dot{Q}_{\text{heat}}) \tag{4}$$

where M_{eng} and C_{eng} are the equivalent thermal mass and the specific heat capacity of the engine cooling system, respectively. $\dot{Q}_{\text{fuel}}$, $\dot{Q}_{\text{exh}}$, $\dot{Q}_{\text{air}}$, and $\dot{Q}_{\text{heat}}$ represent the heat rate released from the combustion process, exchanged through exhaust gases, dissipated by air convection, and delivered for cabin heating, respectively. In particular, $\dot{Q}_{\text{fuel}}$ is calculated using fuel consumption rate and lower heating value (LHV) of the fuel

$$\dot{Q}_{\text{fuel}} = \text{LHV} \cdot \dot{m}_{\text{fuel}} \tag{5}$$

where $\dot{m}_{\text{fuel}}$ is the fuel consumption rate calculated as a function of engine speed (ω_{e}), torque (τ_{e}), and T_{cl}

$$\dot{m}_{\text{fuel}}(\omega_{\text{e}}, \tau_{\text{e}}, T_{\text{cl}}) = \alpha(T_{\text{cl}}) \cdot f_{\text{fuel}}(\omega_{\text{e}}, \tau_{\text{e}}) \tag{6}$$

where $f_{\text{fuel}}(\omega_{\text{e}}, \tau_{\text{e}})$ is the nominal fuel consumption rate and $\alpha(T_{\text{cl}})$ is a multiplier reflecting the fuel consumption sensitivity to the coolant temperature. These functions are adopted from Autonomie[1] software library for a power-split HEV; also see [30] for more details. When T_{cl} is 60 °C, $\alpha = 1.03$ and decreases to $\alpha = 1$ at $T_{\text{cl}} = 100$ °C, at which point the engine is fully warmed up. When T_{cl} is less than 60 °C, α increases, reflecting the engine efficiency degradation at lower coolant and ambient temperatures. For instance, when T_{cl} decreases to 10 °C from 60 °C, α can increase by up to 50%. The experimental validation of the control-oriented models in (3) and (4) can be found in our previous works [29], [30].

III. MPC-Based iPTM of HEVs

The objective of iPTM is to minimize the fuel consumption while enforcing the battery SOC and engine coolant temperature (T_{cl}) constraints in response to the traction and cabin heating demands. In the subsequent numerical examples, the vehicle is considered operating in wintertime when the ambient temperature is −10 °C, and a constant cabin heating power is given by $\dot{Q}_{\text{heat}} = 1.5$ kW. In this section, we first evaluate a conventional MPC with a short receding horizon as the baseline approach. Then, motivated by the limitations of conventional MPC, the MH-MPC is proposed. In all cases, the battery SOC and engine coolant temperature (T_{cl}) are considered as the system states, with battery power (P_{bat}) being the optimization variable.

A. Conventional MPC

As in [20] and [23], the conventional MPC-based strategy for energy management of HEVs is intended to minimize the fuel consumption over a finite prediction horizon, while enforcing the battery SOC charge sustaining constraint. In our case, there are additional constraints on the coolant temperature so the discrete-time optimal control solved at each discrete time instant t becomes

$$\begin{aligned}
\min_{P_{\text{bat}}(i)} \quad & \sum_{i=t}^{t+H-1} \dot{m}_{\text{fuel}}(i)\delta t + \lambda(\text{SOC}(t+H) - \text{SOC}_{\text{r}})^2 \\
\text{s.t. } & \text{SOC}(i+1) = \text{SOC}(i) + \delta t \cdot f_{\text{SOC}}(i) \\
& T_{\text{cl}}(i+1) = T_{\text{cl}}(i) + \delta t \cdot f_{T_{\text{cl}}}(i) \\
& 0.4 \le \text{SOC}(i) \le 0.8 \\
& 40\ ^\circ\text{C} \le T_{\text{cl}}(i) \le 90\ ^\circ\text{C} \\
& T_{\text{cl}}(0) = T_{\text{cl,init}}, \quad \text{SOC}(0) = \text{SOC}_{\text{init}}
\end{aligned} \tag{7}$$

where H is the prediction horizon, and $\delta t = 1$ s is the discrete-time step. We used shorthand notations f_{SOC} and $f_{T_{\text{cl}}}$ for functions used in (3) and (4) in the model described in Section II. In the subsequent simulations, the initial conditions are $\text{SOC}_{\text{init}} = 0.6$ (60%), and $T_{\text{cl,init}} = 50$ °C, representative of a typical scenario where the engine is partially warmed-up. Note that we leave the treatment of cold-start to future publications as it requires additional, specialized modeling and control strategies. The weight in the quadratic penalty term is set to $\lambda = 3$ which promotes charge sustainability. This value has been chosen by trial and error. The reference value for the battery SOC (SOC_{r}) is set to be the same as SOC_{init}. At each time step t, the optimization problem (7) is solved to determine the optimal battery power $[P_{\text{bat}}(t)]$, which informs the required engine power $[P_{\text{eng}}(t)]$ based on (1). Additionally, it is assumed that the engine operates on the curve of optimal operation points (OOP) on the BSFC map. Based on this assumption, for a given $P_{\text{eng}}(t)$, the engine speed and torque are calculated according to the OOP. The optimization problem (7) is solved using MPCTools package [33], which exploits the IPOPT solver [34] and CasADi for numerical optimization. In our simulations, the optimization is warm-started and the solution achieved in the current time step is applied as the initial guess solution for the next iteration. The simulations are performed on a desktop computer with an Intel E-2136@3.30-GHz processor.

To evaluate the performance of the MPC in (7), a driving cycle with the speed profile shown in Fig. 4(a) is considered in this section. This driving cycle is based on the NEDC and includes a combination of city (with multiple stop-and-go) and highway driving. Note that in this section, it is assumed that

[1]Autonomie is a MATLAB/Simulink-based system simulation tool for vehicle energy consumption and performance analysis developed by Argonne National Laboratory (ANL) [6].

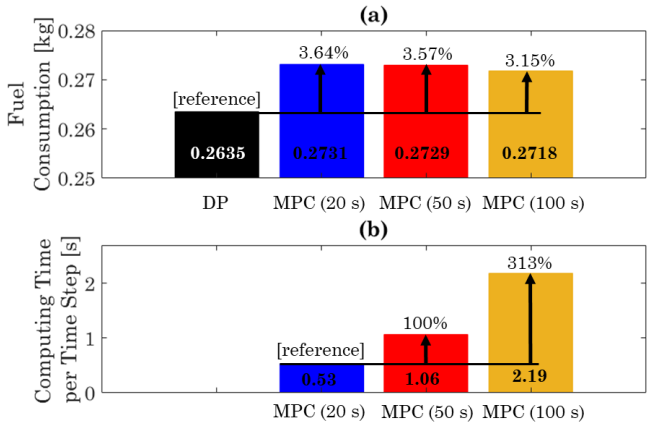

Fig. 3. Simulation results of DP and conventional MPCs with different prediction horizons. (a) Fuel consumption. (b) Average computational time per time step.

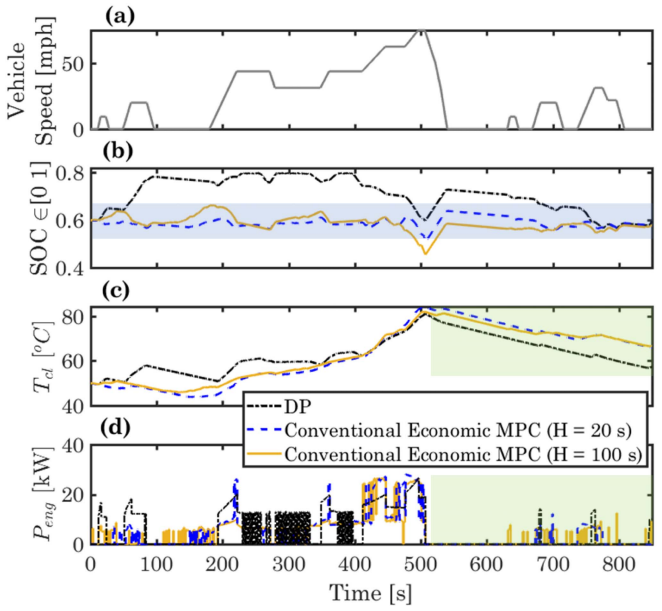

Fig. 4. State trajectories of conventional MPC with different prediction horizons and DP: (a) vehicle speed, (b) SOC, (c) T_{cl}, and (d) engine power.

an accurate prediction of the vehicle speed is available over the prediction horizon, and thus, uncertainties associated with vehicle speed prediction are not taken into consideration. This assumption will be relaxed in Section IV and the sensitivity of the results to the speed preview uncertainty will be investigated.

As the performance of MPC can be affected by the length of the prediction horizon [35], the fuel consumption results for different prediction horizons are summarized in Fig. 3(a). As the benchmark, the optimal solution computed using DP is also shown in Fig. 3. As can be seen, while the fuel consumption decreases as the prediction horizon is extended from 20 to 100 steps, the MPC still consumes 3.15% more fuel than DP. Note that as $\delta t = 1$ s, the time period of one discrete step is 1 s. Fig. 4(b) and (c) show the state trajectories of DP and conventional MPC. One can see that SOC of MPC solution varies in a limited range of $\approx$10%. Furthermore, increasing the prediction horizon has a marginal impact on this narrow variation range. This is because the conventional MPC only has the awareness of the future vehicle speed over the prediction horizon and the quadratic term in the cost function penalizes the SOC deviation from its terminal reference value. DP, on the other hand, has access to the entire driving cycle *a priori*, and thus, the battery can be used more efficiently by expanding the operation range of SOC, as shown in Fig. 4(b). Moreover, as shown in Fig. 4(c), T_{cl} also responds differently with MPC versus DP solution. Exploiting the information about the upcoming long stop (around $t = 100$ to 180 s) before entering the highway, DP increases T_{cl} in advance, thereby avoiding having the coolant temperature drop below its lower limit threshold that can trigger engine idling. The conventional MPC, on the other hand, is able to exploit preview information only over a short horizon, leading the engine to operate within the inefficient coolant temperature range, that is, <50 °C.

Toward the end of the trip, as highlighted in Fig. 4(c), the vehicle exits the highway and starts a city driving phase with low traction power demand and multiple stop-and-go events. Since DP is able to exploit full trip information, it manages to store enough electrical energy in the battery (for traction) and thermal energy in the coolant (for cabin heating) before exiting the highway at around $t = 500$ s, so that the vehicle can reach the end of the trip mainly in full electric mode. This can be seen from the engine power trajectory in Fig. 4(d) showing the engine power is demanded only for few instances after $t = 500$ s. For the MPCs, on the other hand, limited electrical energy has been stored in the battery [Fig. 4(b)], and so the engine is being used more often after $t = 500$ s, resulting in unnecessarily high coolant temperatures by the end of the trip. Note that computing DP solution took about 8 h and hence is not feasible for real-time implementation.

Although the fuel consumption can be reduced with a longer prediction horizon, the MPC computational footprint grows with the length of the prediction horizon as shown in Fig. 3(b). In particular, as the prediction horizon increases from 20 to 100 steps, the computational time increases by 313% on average per time step; thus, longer horizons are prohibitive from the standpoint of real-time implementation.

Based on the results shown in Figs. 3 and 4, the shortcomings of the conventional MPC (7) can be summarized as follows:

1) The quadratic penalty term in the MPC cost function incorporated to enforce the battery charge sustaining constraint limits the operating range of SOC, resulting in inefficient use of the battery. This is the main reason for not observing more substantive improvements in fuel consumption results as the MPC prediction horizon is extended.
2) While the fuel consumption is reduced by extending the MPC prediction horizon, the computational footprint grows to unaffordable levels.
3) Although in this section the vehicle speed (which informs traction power demand) over the prediction horizon is assumed to be known accurately, in the real-world traffic environment, long-term prediction of

the vehicle speed is uncertain. This uncertainty can lead to further degradation of energy efficiency.

To address these challenges, a novel MH-MPC is proposed in Section III-B to address the tradeoff between energy efficiency, computational footprint, and vehicle speed prediction uncertainty.

B. Multihorizon MPC (MH-MPC)

The concept of the proposed MH-MPC is illustrated in Fig. 5. The prediction horizon spans the entire trip, divided into two horizons: 1) a short receding horizon (red window) and 2) a long shrinking horizon (green window). Over the short receding horizon, the vehicle speed preview is assumed to be accurate. Note that for connected vehicles, a high-accuracy short-term prediction of the vehicle speed may be obtained using V2V and V2I communications; see [36] for an example.

Over the long shrinking horizon, an "approximate" vehicle speed preview is assumed to be available. This approximate preview does not require a detailed second-by-second forecast of the vehicle speed. Instead, the time history of the vehicle speed only consists of main traffic events, for example, acceleration and deceleration at signalized intersections and the average cruise speed between the intersections. Note that for a specific road segment with multiple intersections, a long-term vehicle speed preview could be informed by machine learning from the historic traffic data collected from connected vehicles driving through the same corridor; see [25] for an example.

Remark 1: Long-term speed prediction in mixed, uncertain, and dynamic traffic environments is challenging. Real-time route optimization and real-time traffic flow control can complicate the speed and trip time prediction even further. Consequently, it is important to understand the requirements on vehicle speed prediction accuracy, the impact of the associated uncertainties, and acceptable uncertainty bounds to make the iPTM and look-ahead information beneficial for fuel-saving. To that end, Section IV provides statistical analysis to: 1) identify key traffic events and 2) assess the impact of bounded uncertainties in speed prediction on the iPTM results.

The MH-MPC is based on the solution to the following discrete-time optimal control problem:

$$\begin{aligned}
&\min_{P_{\text{bat}}(i)} \sum_{i=t}^{t+N-1} \dot{m}_{\text{fuel}}(i)\Delta t_1 + \sum_{i=t+N}^{t_{\text{end}}} \dot{m}_{\text{fuel}}(i)\Delta t_2 \\
&\text{s.t. } \text{SOC}(i+1) = \text{SOC}(i) + \Delta t_j \cdot f_{\text{SOC}}(i), \quad j \in \{1,2\} \\
&\quad T_{\text{cl}}(i+1) = T_{\text{cl}}(i) + \Delta t_j \cdot f_{T_{\text{cl}}}(i), \quad j \in \{1,2\} \\
&\quad 0.4 \le \text{SOC}(i) \le 0.8 \\
&\quad 40\ ^\circ\text{C} \le T_{\text{cl}}(i) \le 90\ ^\circ\text{C} \\
&\quad 0.99 \times \text{SOC}(0) \le \text{SOC}(t_{\text{end}}) \le \text{SOC}(0) \times 1.01 \\
&\quad T_{\text{cl}}(0) = T_{\text{cl,init}}, \quad \text{SOC}(0) = \text{SOC}_{\text{init}}
\end{aligned} \tag{8}$$

where N is the short receding horizon, t_{end} is the end time of the trip, Δt_1 and Δt_2 are the update periods over the receding and shrinking horizons, respectively, and $j \in \{1,2\}$ is determined as follows:

$$j = \begin{cases} 1, & \textbf{if } i \le t+N-1 \\ 2, & \textbf{if } i \ge t+N. \end{cases} \tag{9}$$

The MH-MPC cost function has two terms:

1) the fuel consumption over the short receding horizon calculated based on accurate vehicle speed preview,
2) an estimate of the fuel consumption over the long shrinking horizon representing the "cost-to-go" of the entire remaining trip beyond the receding horizon.

By adding these two terms, the cost function of MH-MPC reflects the actual fuel consumption over the entire trip. The conventional MPC (7), however, only minimizes the fuel consumption over the receding horizon. Moreover, it can be seen in (8) that a quadratic penalty term in the MH-MPC cost function is no longer needed. This is because the predicted cost-to-go over the shrinking horizon includes an approximation of the SOC evolution until the end of the trip, removing the need for penalizing its deviation from a reference value as in (7). Instead, a terminal constraint is applied to enforce the battery charge sustainability. To improve the feasibility of the optimization problem, the final SOC [i.e., $\text{SOC}(t_{\text{end}})$] is allowed to deviate by $\pm 1\%$ from SOC_{init}. Moreover, due to the inclusion of the cost-to-go term over the shrinking horizon, a precomputed SOC_r trajectory is no longer needed.

To reduce the computational footprint of the MH-MPC over the long shrinking horizon, $\Delta t_2 > \Delta t_1$ is used. The MH-MPC problem is solved every $\Delta t_1 = 1$ s and the first element of the computed control input is applied to the plant. Then, the receding horizon is shifted by Δt_1 and the shrinking horizon is shortened by Δt_1. Note that when the remaining trip time is shorter than the receding horizon length, the multihorizon is no longer needed and there is only one shrinking horizon remaining in the cost function with the sampling time of Δt_1.

While not pursued in this article, note that the model used in the shrinking horizon phase can, in principle, be a lower fidelity model than in the receding horizon phase. Furthermore, alternative integration procedures to Euler's discretization could be implemented in predicting trajectories in the shrinking horizon phase to improve numerical stability.

To study the sensitivity of the MH-MPC to the receding horizon length (N), as well as to the resolution (i.e., sampling time) over the long shrinking horizon (Δt_2), the MH-MPC with different parameters are simulated over the same driving cycle shown in Fig. 4(a). The fuel consumption and the average computational time per time step are summarized in Fig. 6. It can be seen from Fig. 6(a) that decreasing Δt_2 from 20 to 10 s slightly reduces the fuel consumption. Increasing N, however, has a marginal impact on fuel consumption. On the other hand, as shown in Fig. 6(b), different horizon lengths and sampling times lead to different computational footprints. Considering a tradeoff between fuel consumption and computing demands, $N = 5$ s and $\Delta t_2 = 10$ s are selected and used in the remainder of this article. Moreover, the selection of $N = 5$ s makes the availability of accurate speed preview over the receding horizon more reasonable. Note that for the results presented in this section, it is still assumed that a perfect long-term preview is available. However, its accuracy is degraded due to the integration of the continuous-time model with a longer time step.

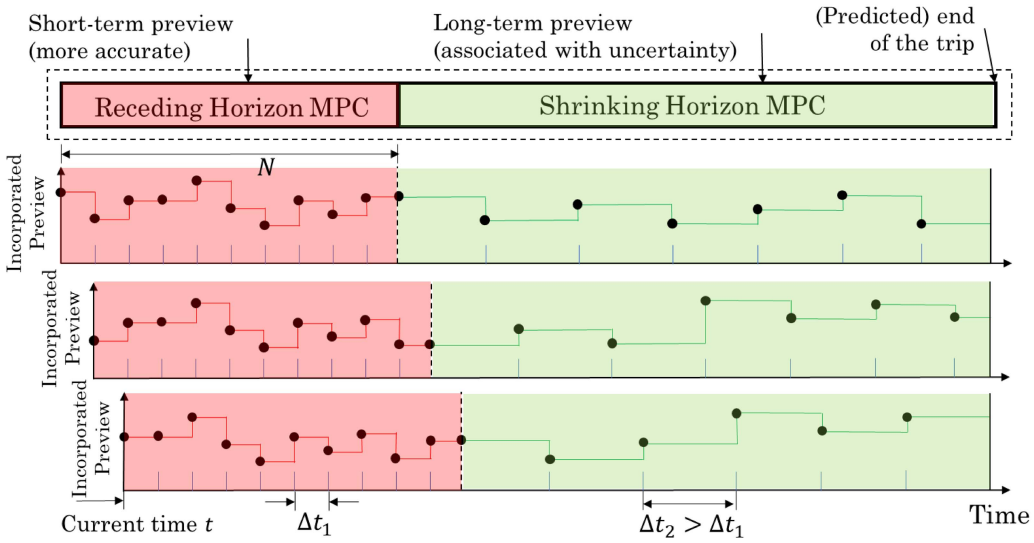

Fig. 5. Concept of MH-MPC with short receding horizon and long shrinking horizon.

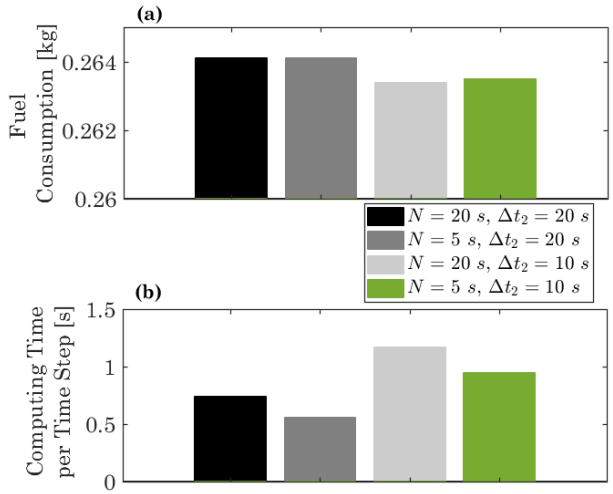

Fig. 6. (a) Fuel consumption and (b) average computational time for different short receding horizons and for different sampling times over the long shrinking horizon.

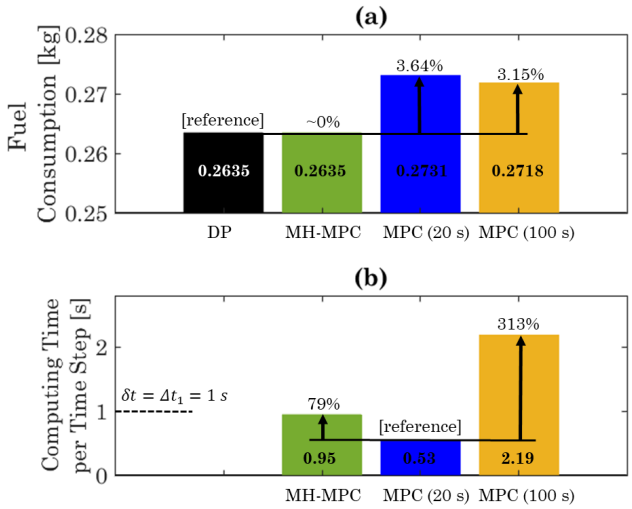

Fig. 7. Simulation results of DP, MH-MPC, and conventional MPC with different prediction horizons. (a) Fuel consumption and (b) average computational time per time step.

Fig. 7 shows the comparison of the results of MH-MPC with DP and conventional MPC. Compared with the conventional MPC, MH-MPC reduces the fuel consumption by more than 3% [Fig. 7(a)], which is similar to DP. By comparing the computational time of MH-MPC and conventional MPC in Fig. 7(b), one can observe that MH-MPC is far less computationally intensive than longer horizon conventional MPC while achieving better performance.

The powertrain trajectories with MH-MPC are shown in Fig. 8 and compared with those of DP and the conventional MPC (with $H = 20$ s). Unlike the conventional MPC, the SOC trajectory of MH-MPC varies over a wider range (>20%) and shows a similar trend with DP. This is because MH-MPC has the awareness of the entire driving cycle and accounts for the cost-to-go beyond the receding horizon. During the first part of the trip, as the initial engine coolant temperature is relatively low, to improve the engine efficiency via engine warm-up, MH-MPC decides to use the engine more frequently and at higher power [Fig. 8(c)] to provide traction power while increasing the coolant temperature. Consequently, the battery is also being charged during this period using the extra engine power. Then, when the vehicle exits the highway (around $t = 540$ s), similar to DP, the vehicle operates mainly in electric mode until the end of the trip ($t = 540$-850 s); see Fig. 8(c). This is possible since the MH-MPC has stored enough thermal energy in the coolant to satisfy the cabin heating toward the end of the trip. Thus, MH-MPC is able to use the engine coolant as thermal energy storage, providing an additional degree of flexibility (in addition to the battery as electrical energy storage) for HEV energy flow optimization.

Remark 2: In this article, the considered driving cycles are relatively short (<1000 s); thus, the end of the optimization horizon is set to be the end of the trip. For longer trips, such a strategy may result in increased computation load for MH-MPC. This issue can be mitigated by: 1) setting the

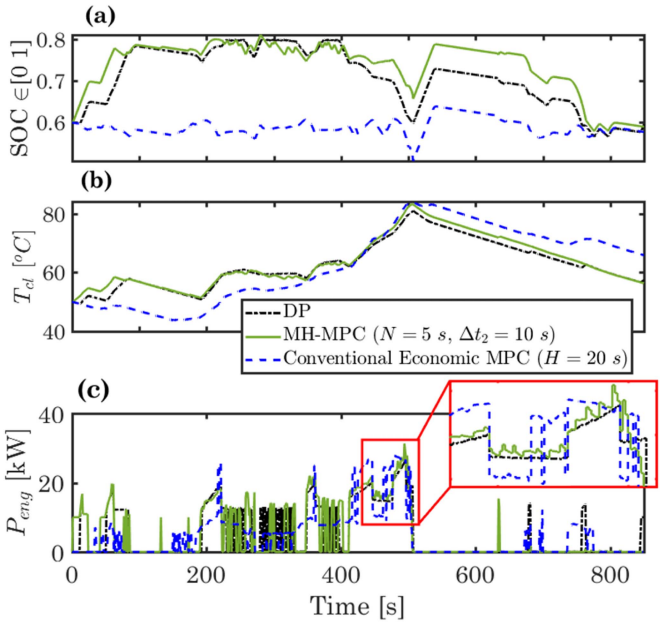

Fig. 8. State trajectories of DP, MH-MPC, and conventional MPC: (a) SOC, (b) T_{cl}, and (c) engine power.

end of the optimization horizon to be the end of a long receding horizon along the trip, and later switching to the shrinking horizon as the vehicle approaches the destination to enforce the terminal constraints; or 2) applying a more intelligent/adaptive sampling procedure over the shrinking horizon to keep the MH-MPC computational footprint at the acceptable level while ensuring that the essential look-ahead information over the long horizon is captured and not missed due to coarse sampling; and finally 3) the use of lower fidelity models for prediction over the shrinking horizon could also be exploited.

IV. Robustness of MH-MPC Against Uncertainties in Vehicle Speed Preview

The benefits of the proposed MH-MPC were studied in Section III under the assumption that the speed preview is known *a priori* over both short- and long-range horizons. In this section, we relax this assumption to investigate the robustness of the MH-MPC to uncertainties associated with vehicle speed preview. As will be shown, this sensitivity analysis helps identify the major traffic events that significantly affect the energy efficiency improvement and hence need to be predicted.

A. Real-World Traffic Simulation Data

To generate the real-world traffic data needed to evaluate the MH-MPC performance, a city corridor was modeled and simulated in the microscopic traffic simulation software VISSIM [37]. The simulated corridor is located on Plymouth Rd., in Ann Arbor, MI, encompassing six intersections as shown in Fig. 9, where the location of each intersection is marked by a black circle. This corridor is about 2.2 miles with two lanes in each direction, connecting the downtown of Ann Arbor to the US-23 highway. Real-world traffic data, including traffic flow volume and signal timing at each intersection, were collected during the rush hour (4:00–5:00 PM) and used to calibrate and validate the VISSIM model as described in our previous publications [29], [38]. A coordinated fixed-time signal timing policy with a cycle length of 150 s has been used in all intersections. This model was run for two and a half hours while the parameters of the traffic model were kept fixed and the traffic congestion-level did not change during the simulation. The speed profiles of 1478 vehicles driving through the entire corridor in the same direction (i.e., entering from the west) were recorded. Note that the total number of vehicles in the traffic traveling through this corridor was larger than 1478 as some vehicles may have entered or exited the corridor at any of the intersections.

B. Sensitivity Analysis of MH-MPC

First, ten vehicles were randomly selected from the pool of 1478 vehicles. For these vehicles, the results of applying MH-MPC are compared with the results of applying DP in Fig. 10. When there is no uncertainty in the speed preview, Fig. 10 shows that for all ten selected vehicles, the MH-MPC achieves a comparable fuel consumption to DP with the difference within 0.9%.

As discussed earlier, uncertainties in the vehicle speed prediction can potentially degrade the fuel consumption. To investigate the impact of speed preview uncertainties on the energy efficiency of MH-MPC, three cases are considered over the long shrinking horizon as follows:

1) *Case I:* Exact vehicle speed is known *a priori*.
2) *Case II:* The only available information is the cruise speed, that is, the speed at which the vehicle is cruising after acceleration from stop and before deceleration to another stop.
3) *Case III:* In addition to the cruise speed (Case II), the spatiotemporal distribution of the vehicle stops at the signalized intersections is known.

Fig. 11 illustrates Cases I and II. It is assumed that the exact ending location of the trip is known *a priori*. In Case II, the vehicle speed over the long shrinking horizon is forecast as constant equal to the last recorded cruise speed. The trip end time is calculated by dividing the remaining distance by the last recorded current cruise speed. When the vehicle comes to stop, the prediction of the trip end time is based on the last recorded cruise speed. Note that as shown in Fig. 11, the cruise speed varies in different segments of the corridor, based on which the estimated trip end time is also recalculated.

Fig. 12 illustrates the vehicle speed forecast in Case III and compares it with Case I, for which the entire driving cycle is known *a priori* over both receding and shrinking horizons. Case III assumes that the stop and departure times at each signalized intersection are known and forecasts the speed between intersections as equal to constant cruise speed in that segment. Note that the predictions of the stop events in Case III can be obtained by analyzing the historical traffic data, as shown in our previous work [25]. In all these three cases, the prediction of the vehicle speed over the short receding

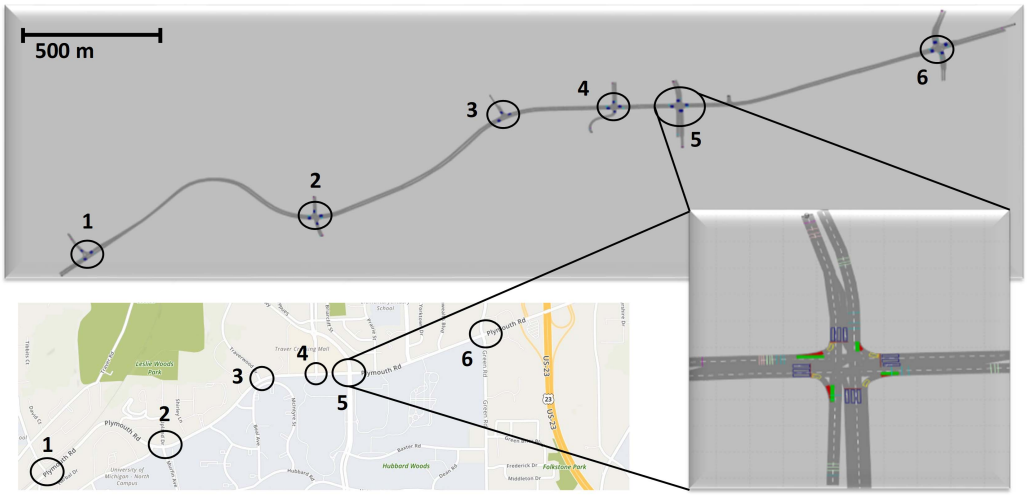

Fig. 9. Plymouth corridor in Ann Arbor used for traffic modeling and simulation.

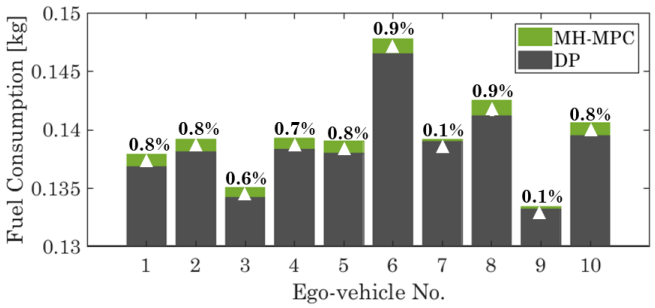

Fig. 10. Fuel consumption results of MH-MPC and offline DP based on ten vehicle speed profiles randomly selected from the Plymouth Rd. driving cycles.

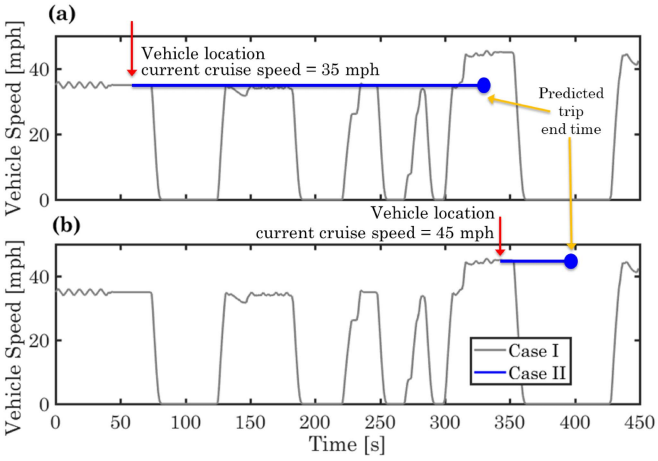

Fig. 11. Case II when compared with Case I and the difference in the incorporated information over the long shrinking horizon of MH-MPC: (a) at around $t = 50$ s, the end time of the trip is estimated based on the known end location and the current cruise speed of 35 mph, and (b) toward the end of the trip at $t = 350$ s, the predicted trip end time is updated based on the remaining distance until the end location and the current cruise speed of 45 mph.

horizon is assumed to be perfect and the trip distance is also known *a priori*.

Among all vehicles traveling through the corridor, 140 vehicles are randomly selected to analyze the performance of

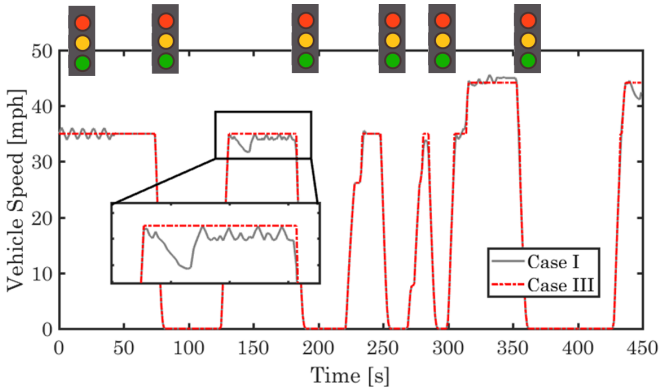

Fig. 12. Case III when compared with Case I and the difference in the incorporated information over the long shrinking horizon of MH-MPC.

the MH-MPC for three cases defined above. While these vehicles have different speed profiles, the initial conditions for T_{cl} and SOC, ambient temperature, and cabin heating demand are the same. Fig. 13 shows the probability density function for the fuel consumption percentage "increase" from Case II and Case III when compared with Case I. Additionally, the conventional MPC with $H = 20$ s is also presented as the benchmark. The average fuel consumption increase of Case II compared with Case I is 1.43%, which is 0.59% better than the conventional MPC on average. It shows that by incorporating the long-term preview via MH-MPC, even with a constant vehicle speed prediction over the long shrinking horizon, the MH-MPC can improve the fuel economy when compared with the conventional MPC.

Comparing Case II and Case III, the fuel consumption is reduced by 1.28% on average and is only 0.15% more on average than in Case I. This suggests that spatiotemporal information about stop events and about cruise speed in intervals between stops can significantly improve fuel economy. The standard deviation of fuel consumption in Case III is 0.30%, which is also lower than in Case II (0.80%).

The state trajectories in three cases for one sample ego-vehicle are shown in Fig. 14. It can be seen that in all three cases, SOC is first pushed toward its upper limit (i.e., 0.8)

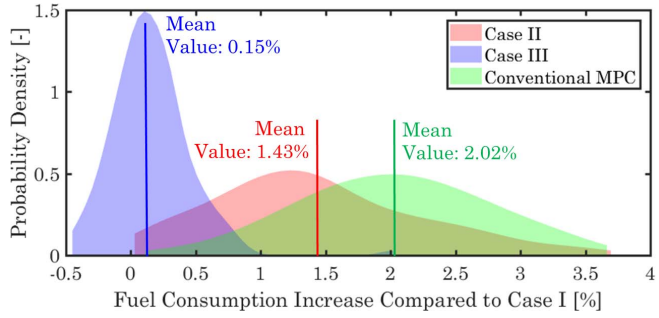

Fig. 13. Probability density function of the fuel consumption increase with uncertain vehicle cruise speed preview.

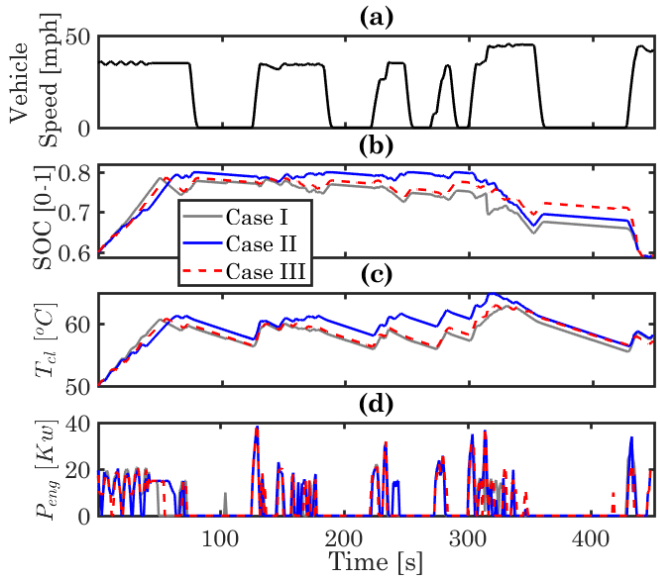

Fig. 14. State trajectories of the three cases evaluated for MH-MPC for one sample ego-vehicle: (a) vehicle speed, (b) SOC, (c) T_{cl}, and (d) engine power (P_{eng}).

while the engine coolant temperature is not warm enough at the beginning of the trip. Note that the SOC constraints are imposed as hard constraints in this article. To avoid the violation of SOC constraints, if $\text{SOC} = \text{SOC}_{\text{max}}$, it is assumed that the friction brake is used instead of the regenerative braking to prevent battery overcharge, meaning the kinetic energy in the braking phase may not be recuperated fully. To fully recuperate the kinetic energy in the braking phase, knowing the upcoming stop event in advance, an optimal controller can command the SOC to decrease using the battery for traction before the brake occurs. This creates spare charge capacity prior to the stop events. Such a desired response is observed for both Cases I and III in Fig. 14(b). For Case II, however, the stop events are not known *a priori* over the long shrinking horizon. As a result, the MH-MPC cannot detect the stop events until the vehicle enters close proximity of the intersection and the stop event becomes visible to the controller within the short receding horizon. Only knowing the upcoming stop event within the short horizon does not provide the controller with enough lead time to discharge the battery proactively, and thus it fails to recuperate the kinetic energy in the braking phase.

TABLE I

MEAN VALUE AND STANDARD DEVIATION OF THE FUEL CONSUMPTION INCREASE RESULTS SHOWN IN FIG. 16

Uncertainty Bound [%]	**0%**	**-10%**	**+10%**	**+20%**	**+30%**	**+40%**
Mean Value [%]	0.15	0.06	0.39	0.87	1.01	1.34
Standard Deviation [%]	0.30	0.32	0.40	0.63	0.68	0.79

As the vehicle approaches the end of the trip, it is also desirable that the controller starts to release the stored electric energy in the battery and the thermal energy in the engine coolant, enabling the vehicle to operate in a more electric mode. Such a favorable response is observed in all cases, even for Case II. Note that for Case II, while the long-term speed prediction has large uncertainty from the beginning, as the vehicles approach the destination, the uncertainty in estimating the trip end time decreases. This allows the MH-MPC for Case II to adjust its actions and release the energy from the battery and the coolant as its awareness of the end of the trip increases.

C. Robustness of MH-MPC

The sensitivity analysis of the MH-MPC in Section IV-B suggested that the preview of stop events and cruise speed can significantly improve the performance of the proposed iPTM strategy based on MH-MPC. To further evaluate the robustness of the MH-MPC to errors in forecasting these, different levels (i.e., from -10% to $+40\%$) of uncertainties are imposed on the "predicted" cruise speed and stop events over the long shrinking horizon as shown in Fig. 15. For instance, assuming the exact location of an intersection is known *a priori*, if the predicted cruise speed is, for example, 10% higher than the actual cruise speed, the predicted stop time is also shifted earlier by 10% when compared with the actual one. Thus, the uncertainty imposed on the cruise speed will affect the predicted stop time at the intersections. To de-couple the cruise speed and vehicle stop time prediction uncertainty from other traffic parameters, here we make several assumptions:

1) The queue length and the number of vehicles between the ego-vehicle and the intersection remain the same while the predicted vehicle cruise speed varies.
2) While the ego-vehicle-predicted cruise speed could be higher or lower than the actual one, it is assumed that the ego-vehicle does not change lane.
3) The departure time from the intersections is determined by the traffic signal timing and the queue conditions at the intersection. Since these two are assumed to remain the same, as shown in the right-hand side of Fig. 15, the predicted departure time from the intersection will not be affected.
4) While the predicted cruise speed varies, the prediction of passing or stopping at the upcoming intersection does not change.

Table I summarizes the statistical results (mean and standard deviation) of the fuel consumption increase compared with the ideal case (Case I), and Fig. 16 shows the probability density

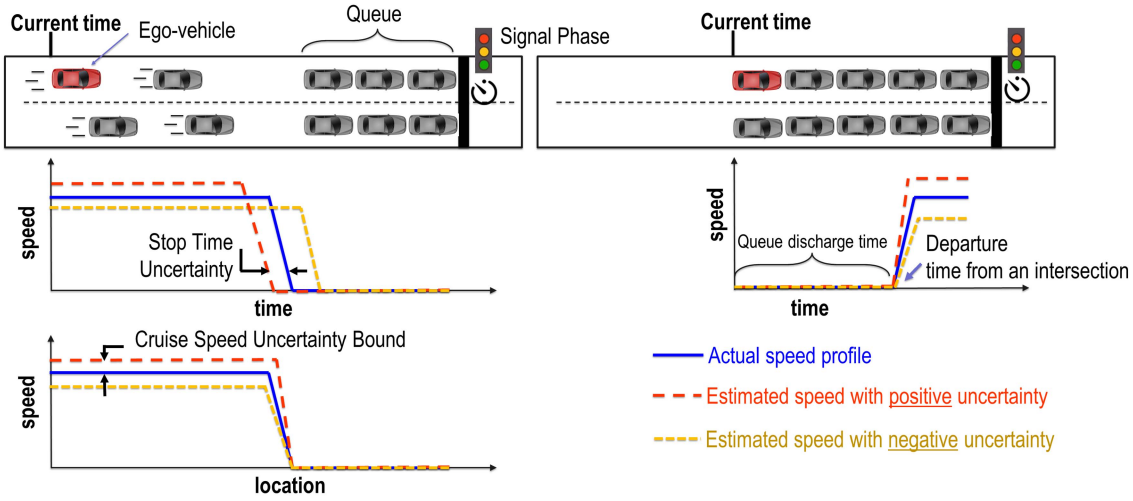

Fig. 15. Concept of imposing the uncertainties on the predicted cruise speed and the stop time.

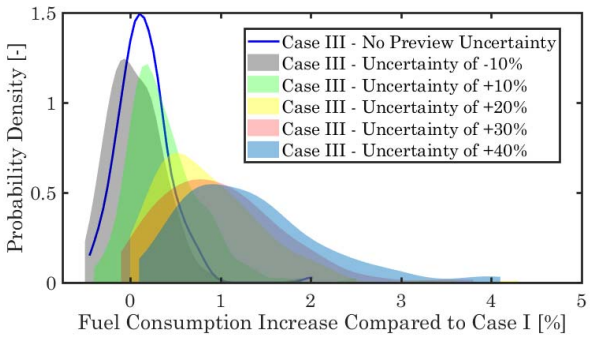

Fig. 16. Probability density function of the fuel consumption increase with different percentages of uncertainties.

functions for different levels of uncertainties. The statistical results are based on the same 140 vehicles considered in the previous subsection. Note that for negative uncertainties, only -10% case is presented, because larger negative uncertainties of the predicted cruise speed make the predicted stop time larger than the departure time. Since the stop time cannot be larger than the departure time, such a case means the vehicle is predicted to pass through the intersection and the associated stop events are not captured.

It can be seen that the average fuel consumption increase percentage, compared with Case I, is negligible when the uncertainties are $\pm 10\%$, and it increases from 0.39% to 1.34%, as the uncertainties increase from $+10\%$ to $+40\%$. As expected, the uncertainty in predicting the actual cruise speed and vehicle stop time degrades the MH-MPC performance. In particular, when the uncertainties are at $+40\%$, the average fuel consumption increases by 1.34%. This observation indicates that when the uncertainties are too large, the benefits of incorporating the stop event predictions could be diminished. Additionally, larger uncertainties lead to a larger standard deviation of fuel consumption increase, indicating higher variability in the fuel consumption results. Fig. 16 shows that the maximum fuel consumption increase is 4.12% when the imposed uncertainties are at $+40\%$.

While the robustness analysis performed in this section focused on one particular type of uncertainty under an assumption that none of the other traffic parameters has changed because of the imposed uncertainty, the results in Fig. 16 are encouraging, suggesting the improvements in fuel consumption are possible despite levels of uncertainties of $\pm 10\%$. As shown in our previous work [25], advanced data-analytic techniques can be applied to improve the accuracy of long-term vehicle speed forecasts, and thus reduce the impact of the associated uncertainties on MPC-based energy management of connected vehicles.

V. Conclusion

In this article, a novel MH-MPC strategy was proposed for integrated systems with dynamics responding over different timescales. The MH-MPC exploits multirange prediction and optimization over a short receding horizon and a long shrinking horizon with different accuracies and resolutions. The MH-MPC estimates the "cost-to-go" over the long shrinking horizon, beyond the conventional receding horizon. This approach makes it appealing for use in mission-based problems where the objective is accomplishing a mission with a limited onboard energy resource. For such systems, the MH-MPC relaxes the requirement for including a terminal penalty term in the receding horizon optimization cost function, allowing to incorporate an economic cost function over the entire prediction horizon. The economic cost function of MH-MPC and long shrinking horizon until the end of the mission enable the energy states to operate on or close to their admissible boundary to improve performance.

This proposed MH-MPC was demonstrated for iPTM of HEVs operating in a connected traffic environment. In such an environment, short- and long-term predictions of the vehicle speed may be obtained using advanced V2V and V2I telematics and incorporated over the receding and shrinking horizons of the MH-MPC. The simulation results of applying MH-MPC to a power-split HEV demonstrated improved performance of the MH-MPC when compared with the conventional MPC with a battery charge sustaining terminal penalty.

Furthermore, in the absence of uncertainties in the vehicle speed forecast, MH-MPC performance was close to that of DP with a deviation of 1%. The MH-MPC performance also surpassed the long-horizon conventional MPC approach, while requiring less computational resources. The sensitivity and robustness of the iPTM strategy to uncertainties in long-term vehicle speed forecasts were also studied. The results suggested that for city driving scenarios, the prediction of the vehicle stop events at signalized intersections and the average cruise speed between intersections are key information that can be leveraged for fuel-saving, even if the prediction is subject to moderate uncertainties.

Our future work will focus on enhancing the MH-MPC robustness using formal algorithmic approaches, as well as estimation and integration of long-term speed preview using advanced data analytic tools started in [25]. We will also consider longer driving cycles, for which an intelligent/adaptive sampling procedure and the use of lower fidelity models over the shrinking horizon may be needed to reduce the computational footprint of MH-MPC. Moreover, to fully quantify the impact of uncertainties in speed prediction on fuel consumption results, the MH-MPC robustness analysis will be expanded to: 1) other types of uncertainties (e.g., imprecisions in trip end time estimation, change of corridor by route optimization algorithm) and 2) longer driving cycles.

ACKNOWLEDGMENT

Hao Wang and Connie Qiu from Ford Motor Company are gratefully acknowledged for their technical comments during the course of this study. Special thanks to Yiheng Feng and Zhen Yang from the University of Michigan for providing real-world traffic data.

REFERENCES

[1] J. Rawlings, D. Mayne, and M. Diehl, *Model Predictive Control: Theory, Computation, and Design*, vol. 2. Madison, WI, USA: Nob Hill Publishing, 2017.

[2] H. Chang and M. Aluko, "Multi-scale analysis of exotic dynamics in surface catalyzed reactions-I: Justification and preliminary model discriminations," *Chem. Eng. Sci.*, vol. 39, no. 1, pp. 37–50, 1984.

[3] S. Skogestad, "Plantwide control: The search for the self-optimizing control structure," *J. Process Control*, vol. 10, no. 5, pp. 487–507, Oct. 2000.

[4] W. C. Clarke, C. Manzie, and M. J. Brear, "Hierarchical economic MPC for systems with storage states," *Automatica*, vol. 94, pp. 138–150, Aug. 2018.

[5] R. Bürger, J. J. R. Damasceno, and K. H. Karlsen, "A mathematical model for batch and continuous thickening of flocculated suspensions in vessels with varying cross-section," *Int. J. Mineral Process.*, vol. 73, nos. 2–4, pp. 183–208, Feb. 2004.

[6] N. Kim, A. Rousseau, D. Lee, and H. Lohse-Busch, "Thermal model development and validation for 2010 Toyota Prius," SAE Technical Paper 2014-01-1784, 2014.

[7] M. R. Amini, H. Wang, X. Gong, D. Liao-McPherson, I. Kolmanovsky, and J. Sun, "Cabin and battery thermal management of connected and automated HEVs for improved energy efficiency using hierarchical model predictive control," *IEEE Trans. Control Syst. Technol.*, vol. 28, no. 5, pp. 1711–1726, Sep. 2020.

[8] M. R. Amini, I. Kolmanovsky, and J. Sun, "Hierarchical MPC for robust eco-cooling of connected and automated vehicles and its application to electric vehicle battery thermal management," *IEEE Trans. Control Syst. Technol.*, vol. 29, no. 1, pp. 316–328, Jan. 2021, doi: 10.1109/TCST.2020.2975464.

[9] J. P. Koeln, H. C. Pangborn, M. A. Williams, M. L. Kawamura, and A. G. Alleyne, "Hierarchical control of aircraft electro-thermal systems," *IEEE Trans. Control Syst. Technol.*, vol. 28, no. 4, pp. 1218–1232, Jul. 2020.

[10] P. Kokotović, H. Khalil, and J. O'reilly, *Singular Perturbation Methods in Control: Analysis and Design*. Philadelphia, PA, USA: SIAM, 1999.

[11] X. Chen, M. Heidarinejad, J. Liu, D. M. de la Peña, and P. D. Christofides, "Model predictive control of nonlinear singularly perturbed systems: Application to a large-scale process network," *J. Process Control*, vol. 21, no. 9, pp. 1296–1305, Oct. 2011.

[12] X. Chen, M. Heidarinejad, J. Liu, and P. D. Christofides, "Composite fast-slow MPC design for nonlinear singularly perturbed systems," *AIChE J.*, vol. 58, no. 6, pp. 1802–1811, Jun. 2012.

[13] M. Ellis, M. Heidarinejad, and P. D. Christofides, "Economic model predictive control of nonlinear singularly perturbed systems," *J. Process Control*, vol. 23, no. 5, pp. 743–754, Jun. 2013.

[14] M. Baldea, P. Daoutidis, and Z. Nagy, "Nonlinear model predictive control of integrated process systems," *IFAC Proc. Volumes*, vol. 43, no. 14, pp. 1040–1045, 2010.

[15] M. A. Brdys, M. Grochowski, T. Gminski, K. Konarczak, and M. Drewa, "Hierarchical predictive control of integrated wastewater treatment systems," *Control Eng. Pract.*, vol. 16, no. 6, pp. 751–767, Jun. 2008.

[16] E. J. Van Henten and J. Bontsema, "Time-scale decomposition of an optimal control problem in greenhouse climate management," *Control Eng. Pract.*, vol. 17, no. 1, pp. 88–96, Jan. 2009.

[17] M. Farina, X. Zhang, and R. Scattolini, "A hierarchical multi-rate MPC scheme for interconnected systems," *Automatica*, vol. 90, pp. 38–46, Apr. 2018.

[18] H. Pangborn, C. Laird, and A. Alleyne, "Hierarchical hybrid MPC for management of distributed phase change thermal energy storage," in *Proc. ACC*, Denver, CO, USA, 2020, pp. 4147–4153.

[19] M. R. Amini, I. Kolmanovsky, and J. Sun, "Two-layer model predictive battery thermal and energy management optimization for connected and automated electric vehicles," in *Proc. 57th IEEE CDC*, Miami Beach, FL, USA, Dec. 2018, pp. 6976–6981.

[20] H. Borhan, A. Vahidi, A. M. Phillips, M. L. Kuang, I. V. Kolmanovsky, and S. Di Cairano, "MPC-based energy management of a power-split hybrid electric vehicle," *IEEE Trans. Control Syst. Technol.*, vol. 20, no. 3, pp. 593–603, May 2012.

[21] M. Debert, G. Yhamaillard, and G. A. Ketfi-Herifellicaud, "Predictive energy management for hybrid electric vehicles-prediction horizon and battery capacity sensitivity," *IFAC Proc. Volumes*, vol. 43, no. 7, pp. 270–275, Jul. 2010.

[22] Q. Hu, M. R. Amini, H. Wang, I. Kolmanovsky, and J. Sun, "Integrated power and thermal management of connected HEVs via multi-horizon MPC," in *Proc. ACC*, Denver, CO, USA, 2020, pp. 3053–3058.

[23] H. Wang, Y. Huang, A. Khajepour, and Q. Song, "Model predictive control-based energy management strategy for a series hybrid electric tracked vehicle," *Appl. Energy*, vol. 182, pp. 105–114, Nov. 2016.

[24] F. Zhang, X. Hu, R. Langari, and D. Cao, "Energy management strategies of connected HEVs and PHEVs: Recent progress and outlook," *Prog. Energy Combustion Sci.*, vol. 73, pp. 235–256, Jul. 2019.

[25] M. R. Amini, Y. Feng, Z. Yang, I. Kolmanovsky, and J. Sun, "Long-term vehicle speed prediction via historical traffic data analysis for improved energy efficiency of connected electric vehicles," *Transp. Res. Rec. J. Transp. Res. Board*, vol. 2674, no. 11, pp. 17–29, Nov. 2020.

[26] N. Kim and A. Rousseau, "Thermal impact on the control and the efficiency of the 2010 Toyota Prius hybrid electric vehicle," *Proc. Inst. Mech. Eng. D, J. Automobile Eng.*, vol. 230, no. 1, pp. 82–92, Jan. 2016.

[27] W. A. Abdelghaffar, M. M. Osman, M. N. Saeed, and A. I. Abdelfatteh, "Effects of coolant temperature on the performance and emissions of a diesel engine," in *Proc. Internal Combustion Engine Division Spring Tech. Conf.*, Rockford, IL, USA, 2002, pp. 187–197.

[28] G. Khoury and D. Clodic, "Method of test and measurements of fuel consumption due to air conditioning operation on the new Prius II hybrid vehicle," *SAE Trans.*, vol. 114, no. 6, pp. 2563–2571, 2005.

[29] M. R. Amini, X. Gong, Y. Feng, H. Wang, I. Kolmanovsky, and J. Sun, "Sequential optimization of speed, thermal load, and power split in connected HEVs," in *Proc. Amer. Control Conf. (ACC)*, Philadelphia, PA, USA, Jul. 2019, pp. 4614–4620.

[30] X. Gong, H. Wang, M. R. Amini, I. Kolmanovsky, and J. Sun, "Integrated optimization of power split, engine thermal management, and cabin heating for hybrid electric vehicles," in *Proc. 3rd CCTA*, Hong Kong, 2019, pp. 567–572.

[31] A. Vahidi and A. Sciarretta, "Energy saving potentials of connected and automated vehicles," *Transp. Res. C, Emerg. Technol.*, vol. 95, pp. 822–843, Oct. 2018.

[32] J. Guanetti, Y. Kim, and F. Borrelli, "Control of connected and automated vehicles: State of the art and future challenges," *Annu. Rev. Control*, vol. 45, pp. 18–40, 2018.

[33] M. Risbeck and J. Rawlings. (2016). *MPCTools: Nonlinear Model Predictive Control Tools for CasADi*. [Online]. Available: https://bitbucket.org/rawlings-group/octave-mpctools
[34] J. A. E. Andersson, J. Gillis, G. Horn, J. B. Rawlings, and M. Diehl, "CasADi: A software framework for nonlinear optimization and optimal control," *Math. Program. Comput.*, vol. 11, no. 1, pp. 1–36, Mar. 2019.
[35] M. Morari and J. H. Lee, "Model predictive control: Past, present and future," *Comput. Chem. Eng.*, vol. 23, nos. 4–5, pp. 667–682, May 1999.
[36] D. Moser, H. Waschl, R. Schmied, H. Efendic, and L. del Re, "Short term prediction of a vehicle's velocity trajectory using ITS," *SAE Int. J. Passenger Cars-Electron. Electr. Syst.*, vol. 8, no. 2, pp. 364–370, Apr. 2015.
[37] *PTV Vissim 9.0 User Manual* PTV AG, PTV Group, Karlsruhe, Germany, 2016.
[38] Z. Yang, Y. Feng, X. Gong, D. Zhao, and J. Sun, "Eco-trajectory planning with consideration of queue along congested corridor for hybrid electric vehicles," *Transp. Res. Rec. J. Transp. Res. Board*, vol. 2673, no. 9, pp. 277–286, Sep. 2019.

Qiuhao Hu received the B.S. and M.S. degrees in naval architecture and ocean engineering from Shanghai Jiao Tong University, Shanghai, China, in 2015 and 2018, respectively. He is currently pursuing the Ph.D. degree with the Department of Naval Architecture and Marine Engineering, University of Michigan, Ann Arbor, MI, USA.

His research interests are in the hybrid electric system, thermal and power management, adaptive control, and optimal control.

Mohammad Reza Amini received the Ph.D. degree in mechanical engineering from Michigan Technological University, Houghton, MI, USA, in 2017.

He is an Assistant Research Scientist with the College of Engineering, University of Michigan, Ann Arbor, MI, with research interests in nonlinear, adaptive, robust, and predictive control theories and their applications to intelligent transportation, automotive, and energy systems.

Ilya Kolmanovsky (Fellow, IEEE) received the Ph.D. degree from the University of Michigan, Ann Arbor, MI, USA, in 1995.

He is a Professor with the Department of Aerospace Engineering, University of Michigan, with research interests in control theory for constrained systems with applications to aerospace and automotive systems.

Jing Sun (Fellow, IEEE) received the Ph.D. degree from the University of Southern California, Los Angeles, CA, USA, in 1989.

She is currently a Professor with the Naval Architecture and Marine Engineering Department, University of Michigan, Ann Arbor, MI, USA. Her research interests include modeling, control, and optimization of dynamic systems, with applications to marine and automotive systems.

Dr. Sun was a recipient of the 2003 IEEE Control System Technology Award. She is a fellow of the National Academy of Inventors, IFAC, and the Society of Naval Architects and Marine Engineers.

Ashley Wiese received the Ph.D. degree in mechanical engineering with The University of Melbourne, Melbourne, Australia, in 2014, focusing on modeling and control of gas turbine air path systems.

He then joined the Walter E. Lay Automotive Engineering Laboratory, University of Michigan, Ann Arbor, MI, USA, as a Research Fellow of the Ford Postdoctoral Program. In 2016, he joined Ford Motor Company, Dearborn, MI, USA, as a Research Engineer in controls and automated systems. His research interest includes optimal and constrained control under uncertainty.

Julia Buckland Seeds received the B.S. and M.S. degrees in aerospace engineering from the University of Cincinnati, Cincinnati, OH, USA, and the Ph.D. degree in electrical engineering from the University of Michigan, Ann Arbor, MI, USA.

She is currently a Technical Leader with the Research and Advanced Controls Engineering Department, Ford Motor Company, Dearborn, MI, where she leads research on modeling and control of advanced technology powertrain systems.